Increasing Octupole Collectivity across the $Z = 64$ Isotopic Chain: B(E3) Values in ^{150}Gd

S. Pascu,[1,2,*] E. Yüksel,[1] Abhishek,[1] P. Stevenson,[1] G. H. Bhat,[3] R. N. Mao,[4] K. Nomura,[5,6] C. Costache,[2] Z. P. Li,[4] N. Mărginean,[2] C. Mihai,[2] T. Naz,[7] Zs. Podolyák,[1] P. H. Regan,[1,8] A. E. Turturică,[2] R. Borcea,[2] M. Boromiza,[2] D. Bucurescu,[2] S. Călinescu,[2] C. Clisu,[2] A. Coman,[2] I. Dinescu,[2] S. Doshi,[9] D. Filipescu,[2] N. M. Florea,[2] A. Gandhi,[2] I. Gheorghe,[2] A. Ionescu,[2] R. Lică,[2] R. Mărginean,[2] R. E. Mihai,[2,10] A. Mitu,[2] N. Nazir,[11] A. Negret,[2] C. R. Niţă,[2] E. B. O'Sullivan,[1,8] C. Petrone,[2] S. E. Poulton,[1,8] J. A. Sheikh,[12] H. K. Singh,[2] L. Stan,[2] S. Toma,[2] G. Turturică,[2] and S. Ujeniuc[2]

[1]*School of Mathematics and Physics, University of Surrey, Guildford GU2 7XH, United Kingdom*
[2]*"Horia Hulubei" National Institute for R&D in Physics and Nuclear Engineering, R-77125 Bucharest-Magurele, Romania*
[3]*Department of Higher Education (GDC Shopian), Jammu and Kashmir 192 303, India*
[4]*School of Physical Science and Technology, Southwest University, Chongqing 400715, China*
[5]*Department of Physics, Hokkaido University, Sapporo 060-0810, Japan*
[6]*Nuclear Reaction Data Center, Hokkaido University, Sapporo 060-0810, Japan*
[7]*Department of Physics, SP College, Cluster University Srinagar, Srinagar 190001, India*
[8]*Marine, Medical and Nuclear Department, National Physical Laboratory, Teddington TW11 0LW, United Kingdom*
[9]*School of Architecture, Technology and Engineering, University of Brighton, Brighton, United Kingdom*
[10]*Institute of Experimental and Applied Physics, Czech Technical University in Prague, Husova 5, Prague, Czech Republic*
[11]*Department of Physics, University of Kashmir, Hazratbal, Srinagar 190 006, India*
[12]*Department of Physics, Islamic University of Science and Technology, Jammu and Kashmir 192 122, India*

(Received 26 July 2024; revised 11 November 2024; accepted 27 January 2025; published 4 March 2025)

An enhanced electric octupole (E3) strength of 45(5) W.u. has been measured for the $3^- \rightarrow 0^+$ transition in ^{150}Gd, providing direct evidence for large octupole collectivity in this nucleus. The value was determined following two sensitive experiments, to measure the mean lifetime of the $J^\pi = 3^-$ level and the weak $E3$ decay branch direct to the ground state. The systematics of the $E3$ strength across the Gd isotopic chain reveals that enhanced octupole collectivity is obtained for ^{150}Gd. The increasing low-lying octupole strength in the Gd isotopes is analyzed with five state-of-the-art theoretical models. It is found to be best reproduced by quasiparticle random phase approximation calculations, providing a good understanding of octupole collectivity in the rare-earth region.

DOI: 10.1103/PhysRevLett.134.092501

Negative-parity states in heavy atomic nuclei were discovered as early as the 1950s and led to the idea that nuclei can assume reflection asymmetric shapes [1,2]. Much experimental and theoretical work has been devoted since then to identifying the regions of the nuclear chart with enhanced octupole collectivity [3,4]. Traditionally, experimental and theoretical studies to search for octupole collectivity have been focused on the neutron-deficient actinides and the neutron-rich lanthanides. This is due to the existence of single-particle orbitals that differ by total and orbital angular momenta $\Delta j = \Delta l = 3$.

The interplay between the quadrupole and octupole degrees of freedom leads to the formation of level sequences characterized by alternating parities [3], connected via strong $E1$ and/or $E3$ transitions. Typically, the negative-parity sequence resides at higher excitation energies relative to the positive-parity sequence and the two structures evolve into a single octupole band only at higher angular momenta. The Gd isotopes serve as a good example of alternating parity structures at low excitation energies, particularly in ^{148}Gd and ^{150}Gd, demonstrating the clear interplay between the quadrupole and octupole modes.

Large electric octupole strength has been found across the nuclear chart around specific proton and neutron numbers N, Z $\simeq$ 34, 56, 88, 134. These large values, often on the order of several tens of Weisskopf units (W.u.), provide compelling evidence for the presence of octupole instability within atomic nuclei. Consequently, they represent a key ingredient, in conjunction with the behavior of negative-parity excited states, that can determine the nature of this instability, specifically, whether it is stable

*Contact author: sorin.pascu@nipne.ro

(the nucleus assumes a permanent octupole shape) or dynamic (the nucleus undergoes octupole vibrations) in character. The best examples of octupole-deformed nuclei have been found in the actinide region [4,5]. Recent measurements of $E3$ strengths in this region have revealed that ^{224}Ra [42(3) W.u] is an example of permanent octupole deformation, while ^{220}Rn (33(4) W.u.) has only octupole instability [6]. Another region where evidence for increased octupole collectivity has been found is the one of rare-earth nuclei centered around quadrupole-deformed Ba isotopes [7–9]. More recently, reduced B(E3) transition probabilities have become available, providing evidence of enhanced octupole collectivity in this region. However, they appear to have an octupole vibrational nature [4,5]. Nevertheless, with values of 48^{+25}_{-34} W.u. and 48^{+21}_{-29} W.u. in ^{144}Ba [10] and ^{146}Ba [11], respectively, these are, to date, the highest B(E3) values in this region. Identifying such regions is of particular importance for the search of the atomic electric moment (EDM) [12]. The best proposed candidates are octupole deformed nuclei, as the quantity behind the EDM, the Schiff moment, is predicted to be enhanced by octupole deformation [13].

The Gd isotopic chain presents some particular characteristics. In ^{146}Gd (N = 82, Z = 64, a quasi-doubly magic nucleus [14,15]), the first excited level is a $J^\pi = 3^-$ state at 1579 keV, analogous to the 2614 keV state in ^{208}Pb. This state decays directly to the ground state via a collective $E3$ transition with B(E3) = 37(4) W.u. [16], similar to the value in ^{208}Pb (34(1) W.u. [17]), and is therefore, interpreted as being an octupole vibrational excitation. In ^{148}Gd (N = 84), a B(E3) strength of 41(6) W.u. was measured in [18], suggesting that the contributions arising from the $f_{7/2} - i_{13/2}$ neutron orbital pair within the N = 82–126 shell increase the B(E3) strength as compared to ^{146}Gd. This trend of increased collectivity is expected to continue for heavier nuclei, as long as deformation plays only a minor role. However, prior to the current work, the corresponding values in ^{150}Gd (N = 86) and ^{152}Gd (N = 88) were absent in the published literature, while the octupole strength in the heavier quadrupole-deformed nuclei ($^{154-160}$Gd) lies much lower, around 15-20 W.u. [19]. In this Letter, we present the first results of two dedicated experiments to extract the low-lying $E3$ strength in the N = 86 isotone, ^{150}Gd, providing direct measurements of the octupole collectivity in this region.

In the present work, the $E3$ transition strength was extracted from measuring the mean lifetime of the $J^\pi = 3^-$ state and the weak direct decay branch to the ground state [19]. Mean lifetime measurements of excited states in ^{150}Gd were conducted using the recoil distance Doppler shift method (RDDS) [20]. The experiment was performed at the Tandem accelerator of IFIN-HH in Bucharest using the ^{140}Ce(^{13}C, 3n) fusion-evaporation reaction and the Cologne-Bucharest plunger device [21]. The beam energy of the ^{13}C ions was 62 MeV, with an average beam intensity

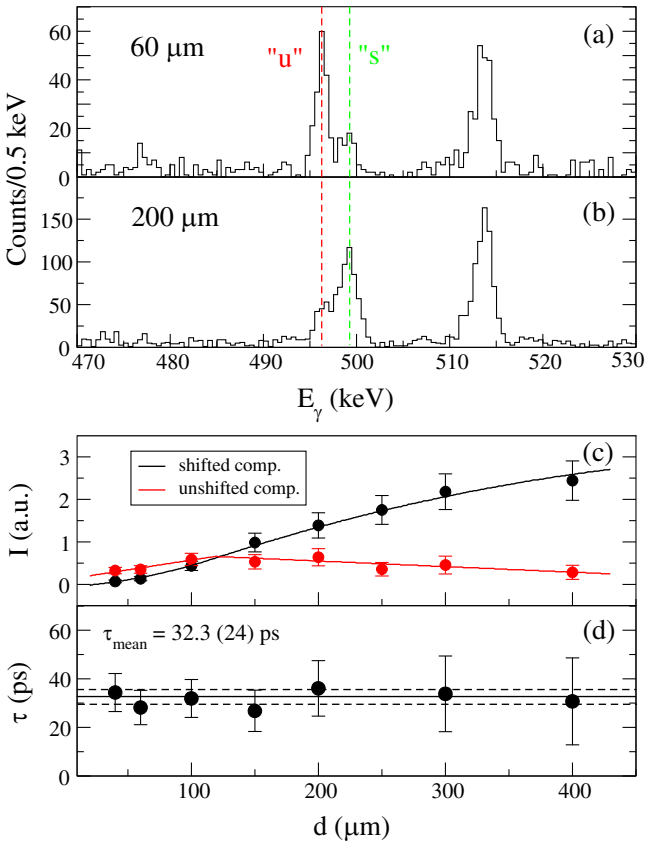

FIG. 1. Shifted ("s") and unshifted ("u") components of the 496 keV γ ray ($3^- \rightarrow 2^+$ transition), measured at 37° relative to the beam axis, at 60 μm [panel (a)] and 200 μm [panel (b)]; (c) Relative intensities of the shifted and unshifted components of the $3^- \rightarrow 2^+$ transition and their corresponding fit with second-degree polynomials; (d) Mean lifetime of the 3^- level as a function of the plunger distance.

of around 5 pnA. The beam was directed onto a thin 0.5 mg/cm^2 ^{140}Ce layer, deposited on a 3 mg/cm^2 Au foil facing the beam. A 4 mg/cm^2 Au stopper foil was used to stop the recoiling ions.

Measurements were taken over ten separate target-stopper foil distances, ranging from 20 μm to 500 μm to cover a broad spectrum of mean lifetimes. The γ rays depopulating the excited states were detected using the ROSPHERE array with the standard configuration [22]. Data measured in HPGe detectors at 37° and 143° were analyzed in coincidence mode with the differential decay curve method (DDCM) [23] (see Ref. [24] for a review). We remind the reader that the $\gamma - \gamma$ coincidence version of the DDCM technique employs a gate on the shifted component of the transition above the level of interest, in order to remove all the feeding contributions, either discrete or unobserved feeding.

Sample γ-ray spectra collected at 60 μm and 200 μm are presented in Figs. 1(a) and 1(b). The spectra show the region around the 496 keV $3^- \rightarrow 2^+$ γ ray, at forward angles (37°), gated above on the shifted component of the

566 keV $5^- \rightarrow 3^-$ γ-ray transition in the backward direction (143°).

In the following, we only discuss the case of the forward-backward matrix, namely the spectra shown in Figs. 1(a) and 1(b). Similar spectra were measured for the other ring-ring combinations and were analyzed independently. The results of the analysis of the relative intensities of the shifted and unshifted components of the 496 keV $3^- \rightarrow 2^+$ γ ray at each distance, for the forward-backward case, are presented in Fig. 1(c). The lifetime determined for each distance is presented in Fig. 1(d), while the average value of all these statistically independent points is used to calculate the mean lifetime of the forward-backward angles combination. The final value ($\tau_{\text{mean}}(3^-) = 32.3(24)$ ps) is obtained as the weighted average of the four mean lifetimes extracted from all possible ring-ring combinations (forward-forward, forward-backward, backward-forward, backward-backward). We note that the horizontal line in Fig. 1(d) represents the value extracted only from the forward-backward combination of detectors as explained above, while the mean lifetime indicated on the figure is the weighted average value extracted from all four possible detector combinations.

A full description of all the results obtained will be given in a forthcoming publication [25]. However, in addition to the mean lifetime of the $J^\pi = 3^-$ state, we also mention here the value obtained for the $J^\pi = 5^-$ state ($\tau_{\text{mean}}(5^-) = 11.0(17)$ ps), for which the $5^- \rightarrow 2^+$ $E3$ strength has also been extracted. The results for the states of interest in ^{150}Gd are summarized in Table I.

Precise branching ratios used to extract transition strengths were determined in this work from a complementary electron capture decay experiment from ^{150}Tb ($Q_{EC} = 4.7$ MeV). The parent nucleus was produced via the ^{147}Sm(^{6}Li, 3n) fusion-evaporation reaction at an incident energy of 33 MeV on a 9.4 mg/cm^2 ^{147}Sm target enriched to 94%. ^{150}Tb features two β-decaying states, a ground state with $J^\pi = (2)^-$, $T_{1/2} = 3.48(16)$ hours, and an isomeric state with $J^\pi = 9^+$, $T_{1/2} = 5.8(2)$ minutes [27]. To extract precise branching ratios of transitions decaying from the 3^- and 5^- states, a 10-minute-on/10-minute-off cycle was employed to enhance the isomer production. Data was collected using the ROSPHERE array in a configuration with 21 HPGe.

The determination of $E3$ branching ratios is usually hampered by two factors: (i) the low intensity carried by these transitions and (ii) the so-called "summation effect." We note that these two effects are correlated, as the low intensity carried by the $E3$ transitions makes the summing of high-intensity γ transitions relevant. The spectrum around the 1134 keV peak ($3^- \rightarrow 0^+$) is presented in Fig. 2(a). This is obtained by gating on the 566 keV, $5^- \rightarrow 3^-$ transition. The peak seen around the energy of 1134 keV has two contributions that must be removed. The first one concerns the summation effect, the case when the two individual γ rays at 638 keV and 496 keV, corresponding to $2^+ \rightarrow 0^+$ and $3^- \rightarrow 2^+$ transitions, are detected in the same detector in the same time window. To estimate the magnitude of this effect, we used the summation observed between transitions 638 ($2^+ \rightarrow 0^+$) and 566 keV ($5^- \rightarrow 3^-$), gated on the 496 keV line ($3^- \rightarrow 2^+$). From this analysis, we could accurately establish the summation contribution to the 1134 keV transition at 37(2)% of the peak area. The second contribution was related to the presence of a so far unobserved transition at an energy of 1132.1 keV. Based on the $\gamma - \gamma - \gamma$ coincidence data analysis, we propose the existence of a new level with an energy of 3068.7 keV. After subtracting these two contributions, the $3^- \rightarrow 0^+$ branching ratio has a value of 0.27(2)% relative to the 496 keV transition. A summary of the uncertainties used in the determination of the branching ratio is given below: (i) ±7% statistical uncertainty; (ii) ±2% systematic uncertainty for the efficiency curve, based on the comparison of the fitted areas of well-known peaks from the decay of ^{150}Tb with the adopted values; (iii) ±1% systematic uncertainty from the angular

TABLE I. Summary of relevant experimental and theoretical results for ^{150}Gd. The state energy (E_i), the mean lifetime (τ), the initial (J_i^π) and final spin (J_f^π), the final state energy (E_f), the multipolarity, the branching ratios (normalized to the most intense γ-ray for each level) (I_γ exp), the conversion coefficient α calculated with the BrIcc code [26], and the experimental transition probabilities in comparison with the calculated values with the QRPA, TDHF, QOCH, m-IBM, and TPSM models (in W.u.) are listed (see text for an explanation of the model labels). Experimental data are taken from [27], except for the mean lifetimes and branching ratios, which are from the current work. The multipolarity of the $5^- \rightarrow 2^+$ transition is assumed in the present measurement as having an $E3$ character based on spin difference.

								B(Eλ)↓ (W.u.)					
E_i [keV]	τ [ps]	J_i^π	J_f^π	E_f [keV]	Mult	I_γ exp	$\alpha(\times 10^{-3})$	Exp	QRPA	TDHF	QOCH	m-IBM	TPSM
1134.30(2)	32.3(24)	3_1^-	2_1^+	638.05(2)	$E1$	100(2)	4.79	$8.7(7) \times 10^{-5}$	⋯	⋯	6.2×10^{-3}	1.7×10^{-3}	3.2×10^{-5}
			0_1^+	0.0	$E3$	0.27(2)	4.39	45(5)	45.9	41.4	13.2	22.5	1.1
1699.91(3)	11.0(17)	5_1^-	4_1^+	1288.42(3)	$E1$	46(1)	7.38	$1.4^{+3}_{-2} \times 10^{-4}$	⋯	⋯	8.7×10^{-3}	3.2×10^{-3}	1.4×10^{-4}
			3_1^-	1134.30(2)	$E2$	100(2)	10.15	18(3)	⋯	⋯	83	52.5	19
			2_1^+	638.05(2)	[E3]	0.10(2)	5.13	53^{+15}_{-12}	⋯	⋯	25.3	28	2.4

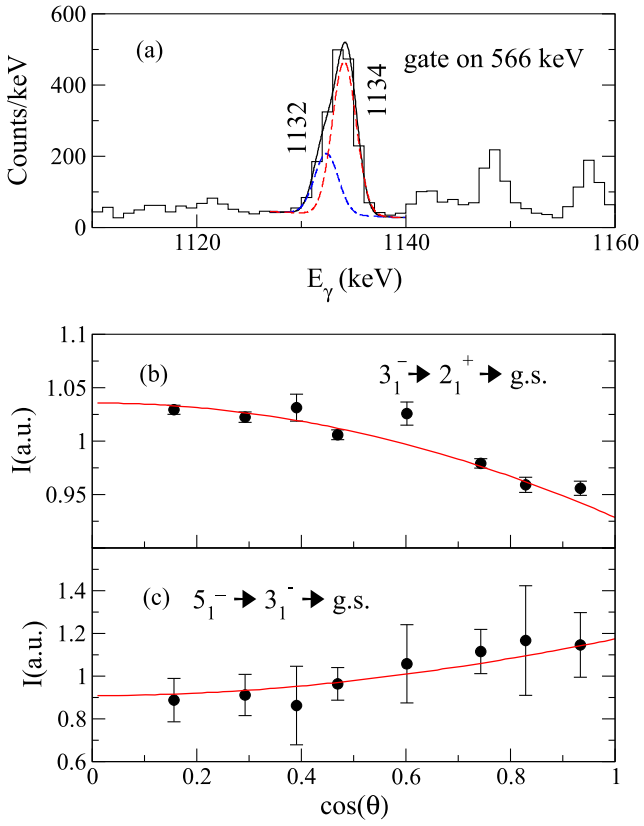

FIG. 2. (a) Relevant part of the γ-ray spectrum illustrating the region around the 1134 keV transition ($3^- \rightarrow 0^+$), gated by the 566 keV ($5^- \rightarrow 3^-$) transition. A fit of the two components is shown: 1132 (blue) and 1134 keV (red); (b) and (c) angular correlations of the $3^- \rightarrow 2^+ \rightarrow$ g.s. and $5^- \rightarrow 3^- \rightarrow$ g.s. experimental (full points) and theoretical (red line) angular correlations, assuming $E1$-$E2$ and $E2$-$E3$ pure multipolarities, respectively. Angular correlations are normalized to the $6_2^+ \rightarrow 4_1^+ \rightarrow 2_1^+$ cascade.

correlations. Due to the spherical geometry of ROSPHERE, small angular correlation attenuation factors have been calculated, amounting to less than 1% for the cascades of interest. No other summing out of the 1134 keV transition with other intense γ rays was taken into account.

Angular correlation measurements were performed to verify the multipolarity of the 1134 keV transition. HPGe detectors were arranged in eight different groups according to their relative angle. The results of this analysis are presented in Figs. 2(b) and 2(c) for the 496 keV $3^- \rightarrow 2^+$ transition (3-2-0 spin sequence) and 1134 keV $3^- \rightarrow 0^+$ transition (5-3-0 spin sequence), respectively. The solid lines are the theoretical angular correlation curves for pure multipolarities, supporting the spin assignments.

With the high level of statistics from the present experiment, we were also able to extract the intensity of the $E3$ $5^- \rightarrow 2^+$ transition. In the Adopted file of ENSDF for mass 150 [27], this transition is seen with an intensity of 15(3)% relative to the 566 keV transition. We observe a considerably weaker intensity for this transition, amounting to only 0.10(2)% relative to the 566 keV intensity. With the mean lifetime measured in the RDDS experiment and the old intensity value, an $E3$ strength larger than 6100 W.u. would result. Using our value for this branching ratio, we obtain an $E3$ strength of 53^{+15}_{-12} W.u. This $E3$ value has a comparable strength to that of the $3^- \rightarrow 0^+$ transition, in line with the expectation of an octupole phonon coupled with the 2^+ state.

The B(E3)↓ value of 45(5) W.u. for the $3^- \rightarrow 0^+$ transition in ^{150}Gd is the highest and the most precise octupole strength measured in the rare-earth region [19] for reduced electric octupole transition probabilities starting from the ground state. This suggests that ^{150}Gd isotope possesses an enhanced octupole collectivity, rivaled only by the values in deformed ^{144}Ba and ^{146}Ba, although these values have been determined with large uncertainties [10,11].

In Fig. 3(a), we present the systematics of known experimental octupole strength in the rare-earth region

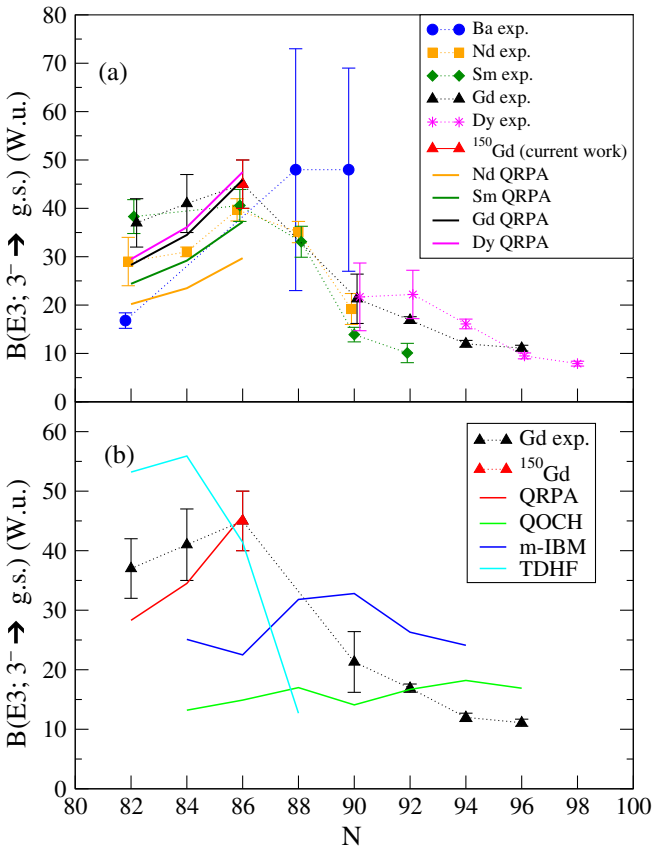

FIG. 3. (a) The systematics of measured (full symbols) B(E3)↓ $3^- \rightarrow 0^+$ strength in the Ba-Dy region (red triangle is from the current work). In addition, the results of the QRPA model for the Nd, Sm, Gd, and Dy isotopic chains are presented (full lines) in the N = 82–86 region; (b) Experimental B(E3)↓ $3^- \rightarrow 0^+$ for Gd isotopes are compared with state-of-the-art theoretical calculations.

between Ba (Z = 56) and Dy (Z = 66) isotopes [27–40]. We have added also in Fig. 3(a) the results of the QRPA calculation for the Nd-Dy isotopic chains, which will be discussed later. For the moment, we focus the discussion on the experimental part. The values generally increase from N = 82 toward the "octupole driving number" N = 88, then decrease toward heavier isotopes. In deformed nuclei, it is believed that a reduction in the B(E3) values could arise because the $E3$ strength is no longer concentrated in the lowest octupole band [5]. A lack of precise data makes it difficult to quantify the location of the maximum octupole strength for each isotopic chain, but in general, the maximum appears to be realized at N = 86. Nevertheless, the result for ^{150}Gd stands out and proposes a very strong octupole collectivity for Gd isotopes, which has not been recognized so far in this region.

Comprehensive theoretical calculations have been conducted using a diverse array of advanced theoretical models, each grounded in distinct assumptions: (i) Fully self-consistent Quasi-particle Random Phase Approximation (QRPA) calculations [41,42] were performed employing the Skyrme-type SkX interaction [43], with the assumption of spherical symmetry. (ii) In the case of the time-dependent Hartree-Fock (TDHF) model, the SkM* Skyrme interaction was used [44] to evaluate both the ground state and the octupole state. The octupole state was derived by exciting the spherical or deformed ground state via an octupole boost [45], and the B(E3) values were determined by fitting a Lorentzian to the lowest-lying peak in the strength function. (iii) The quadrupole-octupole collective Hamiltonian (QOCH) serves as a collective model that expresses the collective Hamiltonian as the sum of vibrational kinetic energy, rotational kinetic energy, and the collective potential [46,47]. (iv) The mean-field mapped interacting boson model (m-IBM) employs a mapping procedure to derive the model parameters [48] from the bosonic potential energy surface to the Hartree-Fock-Bogoliubov (HFB) framework grounded in Gogny-EDF calculations [49]. (v) Lastly, the triaxial projected shell model (TPSM) represents a semi-microscopic approach that incorporates a deformed basis achieved through the use of the triaxial Nilsson potential, thereby explicitly introducing the triaxial degree of freedom [50].

A comparison of experimental and theoretical transition strengths for the states of interest is shown in Table I. For the QRPA and the TDHF, only the transition strength from the ground state can be calculated, while for the other models, the full set of transition strengths is shown. Interestingly, among all five theoretical models, the QRPA reproduces well the experimental $B(E3; 3^- \rightarrow 0^+)$ transition strength, with a value of 45.9 W.u. as compared to the measured 45(5) W.u. In the present QRPA calculations, the B(E3) values are calculated by summing over the contributions of all proton configurations. The first 3^- states in Gd isotopes display collectivity, and the main configurations that produce the major contribution for the first 3^- state in ^{150}Gd are the two quasi-particle configurations $\pi 1h_{11/2}$-$\pi 2d_{5/2}$ and $\pi 1h_{11/2}$-$\pi 1g_{7/2}$, with 64% and 5%, respectively. The TDHF calculation for the $E3$ strength is also in reasonable agreement with the experimental value, with a calculated strength of 41.4 W.u. We note, however, that the calculated 3^- energy is much lower than the experimental value ($E_{exp} = 1134$ keV, $E_{TDHF} = 410$ keV). For the other three theoretical models, the predicted values are 22.5 W.u, 13.2 W.u., and 1.1 W.u., for the m-IBM, QOCH, and TPSM models, respectively, thereby severely underestimating the experimental value.

The QRPA, TDHF, QOCH, and m-IBM models have also been employed to study the systematics of $E3$ strength across the Gd nuclei. In addition, the QRPA is employed to calculate the B(E3) values across several isotopic chains, from Nd to Dy, in the N = 82–86 region, where the spherical approximation remains valid. These results are presented in Fig. 3(a), while the results only for the Gd isotopes are given in Fig. 3(b). In each isotopic chain studied in this work, the B(E3) strength increases with increasing neutron number, as the contribution from neutron transitions also start to increase. Moreover, for constant N, the B(E3) strength is seen to increase with increasing Z, while going from Nd to Dy isotopes, in good agreement with the available experimental trends. We note that the $E3$ strength increase from Gd to Dy is relatively small, signaling a saturation of the B(E3) values toward the middle of the Z = 50–82 shell. Although we do not present these results here, further calculations for Er and Yb nuclei show that the maximum octupole collectivity is obtained for Dy nuclei.

Coming back to the discussion on Gd isotopes, it is clear that QRPA is not only predicting a correct value for the $E3$ strength in ^{150}Gd, but it also reproduces the decreasing trend toward ^{146}Gd. We note that the QRPA model used in our calculations is more suited for describing spherical nuclei. Theoretical calculations using the HFB method [51] indicate that ^{146}Gd is spherical, and quadrupole deformation increases gradually with increasing neutron number. Nonetheless, the quadrupole deformation β_2 values are not high and obtained around 0.15 for ^{150}Gd using the SkX interaction, allowing the QRPA model to remain valid, to a good approximation, for the first 3^- state calculations. Therefore, applying the same model to a highly deformed nucleus, for instance, ^{152}Gd, results in an even higher B(E3) value (59 W.u.) compared to ^{150}Gd. We note that this value is in line with the experimental data extracted for ^{152}Gd from inelastic scattering experiments [19] (52(17) W.u.). However, this procedure is model dependent, and as such, the experimental value was not included in Fig. 3.

The TDHF model produces a maximum octupole collectivity for ^{148}Gd, with a sharp decrease while going to ^{152}Gd. All the other models predict a relatively constant

behavior of the $E3$ strength, in stark contrast to the experimental situation.

A lower $E3$ strength is predicted by the QOCH, m-IBM, and TPSM models also for the $5^- \rightarrow 2^+$ transition (53^{+15}_{-12} W.u in the experiment). The largest value is 28 W.u. in the m-IBM, but still a factor of almost 2 lower than the experimental data. We note, however, that the $E1$ strengths are well reproduced by the TPSM. All calculated values are summarized in Table I, and indicate that describing the octupole collectivity remains a challenge for theoretical calculations.

In conclusion, we provide the first direct evidence for increased octupole collectivity across the $Z = 64$ Gd isotopic chain. This result was made possible using a combination of mean lifetime measurements of the low-lying negative-parity states with the recoil distance Doppler shift method, as well as a precise determination of the weak $3^- \rightarrow 0^+$ and $5^- \rightarrow 2^+$ transitions. The extracted $B(E3; 3^- \rightarrow \text{g.s.})$ strength is crucial for defining the boundaries of strong octupole collectivity in the rare-earth region, believed so far to be realized mainly in the deformed Ba isotopes. The comparison with five state-of-the-art theoretical calculations indicates that, although a complete description of the octupole collectivity in this region is lacking, the QRPA and TDHF models come very close to describing the $E3$ strength in the spherical region of the Gd isotopic chain. The current findings pave the way for further examining the development of octupole strength in the rare-earth nuclei, in particular in ^{152}Gd. Moreover, the enhanced $E3$ strength measured in this work provides a strong argument to search for double octupole states. We note that in ^{150}Gd, the level at 2306.2 keV [27] with $J^\pi = (5^-, 6^+)$ decays predominantly toward negative-parity states. Future Coulomb excitation experiments with radioactive beams could shed more light on this.

Acknowledgments—We appreciate the excellent work of the Tandem accelerator team in delivering a high-intensity and stable beam throughout the two experiments. P. H. R. acknowledges support from the UK National Measurements System Programmes Unit of the UK's Department for Science, Innovation and Technology (DESIT). This work is supported by the UK STFC under Grants No. ST/V001108/1 and No. ST/Y000358/1 and by the Romanian Nucleu Project No. PN 23 21 01 02. This project has received funding from the European Union's Horizon Europe Research and Innovation programme under Grant Agreement No. 101057511 (EUROLABS).

[1] F. Asaro, F. Stephens Jr., and I. Perlman, Phys. Rev. **92**, 1495 (1953).
[2] F. S. Stephens, Jr., F. Asaro, and I. Perlman, Phys. Rev. **100**, 1543 (1955).
[3] P. A. Butler and W. Nazarewicz, Rev. Mod. Phys. **68**, 349 (1996).
[4] P. A. Butler, J. Phys. G **43**, 073002 (2016).
[5] P. A. Butler, Proc. R. Soc. A **476**, 20200202 (2020).
[6] L. P. Gaffney, P. A. Butler, M. Scheck, A. B. Hayes, F. Wenander, M. Albers, B. Bastin, C. Bauer, A. Blazhev, S. Bönig *et al.*, Nature (London) **497**, 199 (2013).
[7] W. R. Phillips, I. Ahmad, H. Emling, R. Holzmann, R. V. F. Janssens, T.-L. Khoo, and M. W. Drigert, Phys. Rev. Lett. **57**, 3257 (1986).
[8] W. Urban, M. A. Jones, J. L. Durell, M. Leddy, W. R. Phillips, A. G. Smith, B. J. Varley, I. Ahmad, L. R. Morss, M. Bentaleb *et al.*, Nucl. Phys. **A613**, 107 (1997).
[9] G. A. Leander, W. Nazarewicz, P. Olanders, I. Ragnarsson, and J. Dudek, Phys. Lett. **152B**, 284 (1985).
[10] B. Bucher, S. Zhu, C. Y. Wu, R. V. F. Janssens, D. Cline, A. B. Hayes, M. Albers, A. D. Ayangeakaa, P. A. Butler, C. M. Campbell *et al.*, Phys. Rev. Lett. **116**, 112503 (2016).
[11] B. Bucher, S. Zhu, C. Y. Wu, R. V. F. Janssens, R. N. Bernard, L. M. Robledo, T. R. Rodríguez, D. Cline, A. B. Hayes, A. D. Ayangeakaa *et al.*, Phys. Rev. Lett. **118**, 152504 (2017).
[12] T. E. Chupp, P. Fierlinger, M. J. Ramsey-Musolf, and J. T. Singh, Rev. Mod. Phys. **91**, 015001 (2019).
[13] J. Dobaczewski, J. Engel, M. Kortelainen, and P. Becker, Phys. Rev. Lett. **121**, 232501 (2018).
[14] Y. Nagai, J. Styczen, M. Piiparinen, P. Kleinheinz, D. Bazzacco, P.v Brentano, K. O. Zell, and J. Blomqvist, Phys. Rev. Lett. **47**, 1259 (1981).
[15] W. H. Long, T. Nakatsukasa, H. Sagawa, J. Meng, H. Nakada, and Y. Zhang, Phys. Lett. B **680**, 428 (2009).
[16] P. Kleinheinz, M. Ogawa, R. Broda, P. J. Daly, D. Haenni, H. Beuscher, and A. Kleinrahm, Z. Phys. A At. Nucl. **286**, 27 (1978).
[17] M. J. Martin, Nucl. Data Sheets **108**, 1583 (2007).
[18] Zs. Podolyák, P. G. Bizzeti, A. M. Bizzeti-Sona, S. Lunardi, D. Bazzacco, A. Dewald, A. Algora, G. de Angelis, E. Farnea, A. Gadea, D. R. Kasemann *et al.*, Eur. Phys. J. A **17**, 29 (2003).
[19] T. Kibedi and R. H. Spear, At. Data Nucl. Data Tables **80**, 35 (2002).
[20] A. Dewald, S. Harissopulos, and P. von Brentano, Z. Phys. A At. Nucl. **334**, 163 (1989).
[21] C. Mihai, Horia Hulubei National Institute for R&D in Physics and Nuclear Engineering, Ph.D. thesis, 2011.
[22] D. Bucurescu, I. Căta-Danil, G. Ciocan, C. Costache, D. Deleanu, R. Dima, D. Filipescu, N. Florea, D. G. Ghiţă, T. Glodariu, M. Ivaşcu *et al.*, Nucl. Instrum. Methods Phys. Res., Sect. A **837**, 1 (2016).
[23] G. Böhm, A. Dewald, P. Petkov, and P. von Brentano, Nucl. Instrum. Methods Phys. Res., Sect. A **329**, 248 (1993).
[24] A. Dewald, O. Möller, and P. Petkov, Prog. Part. Nucl. Phys. **67**, 786 (2012).
[25] S. Pascu *et al.*, companion paper, Phys. Rev. C **111**, 034302 (2025).
[26] T. Kibédi, T. W. Burrows, M. B. Trzhaskovskaya, P. M. Davidson, and C. W. Nestor, Jr., Nucl. Instrum. Methods Phys. Res., Sect. A **589**, 202 (2008).
[27] S. K. Basu and A. A. Sonzogni, Nucl. Data Sheets **114**, 435 (2013).
[28] J. Chen, Nucl. Data Sheets **146**, 1 (2017).

[29] T. Belgya, R. A. Gatenby, E. M. Baum, E. L. Johnson, D. P. DiPrete, S. W Yates, B. Fazekas, and G. Molnár, Phys. Rev. C **52**, R2314 (1995).
[30] A. A. Sonzogni, Nucl. Data Sheets **93**, 599 (2001).
[31] Yu. Khazov, A. Rodionov, and G. Shulyak, Nucl. Data Sheets **136**, 163 (2016).
[32] N. Nica, Nucl. Data Sheets **117**, 1 (2014).
[33] M. J. Martin, Nucl. Data Sheets **114**, 1497 (2013).
[34] C. W. Reich, Nucl. Data Sheets **110**, 2257 (2009).
[35] C. W. Reich, Nucl. Data Sheets **113**, 2537 (2012).
[36] N. Nica, Nucl. Data Sheets **141**, 1 (2017).
[37] N. Nica, Nucl. Data Sheets **176**, 1 (2021).
[38] N. Nica, Nucl. Data Sheets **195**, 1 (2024).
[39] B. Singh and J. Chen, Nucl. Data Sheets **147**, 1 (2018).
[40] R. H. Spear, W. J. Vermeer, S. M. Burnett, G. J. Cyapong, and C. S. Lim, Aust. J. Phys. **42**, 345 (1989).
[41] G. Colò and X. Roca-Maza, arXiv:2102.06562.
[42] G. Colò, L. Cao, N. Van Giai, and L. Capelli, Comput. Phys. Commun. **184**, 142 (2013).
[43] B. A. Brown, Phys. Rev. C **58**, 220 (1998).
[44] J. Bartel, P. Quentin, M. Brack, C. Guet, and H.-B. Hakansson, Nucl. Phys. **A386**, 79 (1982).
[45] Abhishek, P. Stevenson, Y. Shi, E. Yüksel, and A. S. Umar, Comput. Phys. Commun. **301**, 109239 (2024).
[46] P. Marević, J.-P. Ebran, E. Khan, T. Nikšić, and D. Vretenar, Phys. Rev. C **97**, 024334 (2018).
[47] S. Y. Xia, H. Tao, Y. Lu, Z. P. Li, T. Nikšić, and D. Vretenar, Phys. Rev. C **96**, 054303 (2017).
[48] K. Nomura, R. Rodríguez-Guzmán, and L. M. Robledo, Phys. Rev. C **92**, 014312 (2015).
[49] J. Decharge, M. Girod, and D. Gogny, Phys. Lett. B **55**, 361 (1975).
[50] T. Naz, G. H. Bhat, S. Jehangir, S. Ahmad, and J. A. Sheikh, Nucl. Phys. **A979**, 1 (2018).
[51] P. Marević, N. Schunck, E. Ney, R. Navarro Pérez, M. Verriere, and J. O'Neal, Comput. Phys. Commun. **276**, 108367 (2022).